Soft Matter

PAPER

View Article Online
View Journal

Cite this: DOI: 10.1039/d0sm01516d

Adhesion of a tape loop†

Theresa Elder, [a] Timothy Twohig, [b] Harmeet Singh [c] and Andrew B. Croll *[ab]

Received 20th August 2020,
Accepted 2nd November 2020

DOI: 10.1039/d0sm01516d

rsc.li/soft-matter-journal

In this work, we revisit experimentally and theoretically the mechanics of a tape loop. Using primarily elastic materials (polydimethylsiloxane, PDMS, or polycarbonate, PC) and confocal microscopy, we monitor the shape as well as the applied forces during an entire cycle of compression and retraction of a half-loop compressed between parallel glass plates. We observe distinct differences in film shape during the cycle; points of equal applied force or equal plate separation differ in shape upon compression or retraction. To model the adhesion cycle in its entirety, we adapt the 'Sticky Elastica' of [T. J. W. Wagner *et al., Soft Matter*, 2013, **9**, 1025–1030] to the tape loop geometry, which allows a complete analytical description of both the force balance and the film shape. We show that under compression the system is generally not sensitive to interfacial interactions, whereas in the limit of large separation of the confining parallel plates during retraction the system is well described by the peel model. Ultimately, we apply this understanding to the measurement of the energy release rate of a wide range of different cross-linker ratio PDMS elastomer half-loops in contact with glass. Finally, we show how the model illuminates an incredibly simple adhesion measurement technique, which only requires a ruler to perform.

1 Introduction

When attaching one flat object to another, say a poster to a wall, it is not uncommon to use a loop of tape. Bending a flat piece of adhesive tape 180° such that the sticky side of the tape points outwards is a simply created solution, however, the mechanics of the attachment process is more complex. An example of this complexity can be seen when a newly made tape loop is gently placed on a horizontal surface (Fig. 1a). The loop will retain its original circular cross-section indefinitely (a fact which is independent of the particular type of tape used or the substrate). If the loop is compressed, it will deform into an elongated shape which is relatively flat along the horizontal surface and highly curved at the ends (see Fig. 1b). When the compressive pressure is released, the shape opens slightly but does not return to its original cylindrical shape (Fig. 1c).

The cycle is hysteretic; adhesion is present but is not enough to pull the system into equilibrium. Perhaps the observation that equilibrium does not govern the shape of the tape loop is easily ignored because tapes, like all pressure sensitive adhesives, are designed to dissipate energy. Loss, of course, means the system will be path dependent. However, we show here that the same effect is observed even with the use of low loss materials like polycarbonate.

The ubiquity of the tape loop would also suggest that it might be useful for quantifying adhesion. This could only be the case if a loop were to find equilibrium when placed on a surface. In this case, the loop would act like a fluid drop and flow into a particular contact shape (a contact angle could be measured if it were a fluid). The shape would change from one surface to another and could therefore be used to discuss adhesion. Unfortunately, because the loop shape depends on history it is of no use in measurement, and its use to solve the problem of attaching one flat object to another can only be determined by an Edisonian process (*e.g.* if it doesn't work at first, use more tape loops).

In this work we experimentally examine the attachment and detachment process using an idealized half-loop geometry and several different polymeric thin films chosen to vary the amount of energy loss at the interface. One of our main observations is that the hysteresis in shape is a general geometric feature of any adhesive loop, not simply the product of energy dissipation. We go on to show how the 'Sticky Elastica' model can be adapted to this geometry and provide theoretical insight, enabling the loop to be reliably used as an adhesion measurement system. We verify the usefulness of the loop by measuring the adhesive energy release rate for various polydimethylsiloxane (PDMS) elastomer formulations. Finally, we use the model to identify an incredibly simple method

[a] *Materials and Nanotechnology, North Dakota State University, Fargo, USA*
[b] *Department of Physics, North Dakota State University, Fargo, USA. E-mail: andrew.croll@ndsu.edu; Tel: 413-320-3810*
[c] *Institute of Mathematics, École Polytechnique Fédérale de Lausanne, MA C1 612 (Bâtiment MA), Station 8, CH-1015 Lausanne, Switzerland*

† Electronic supplementary information (ESI) available: Details of calculations in the text. See DOI: 10.1039/d0sm01516d

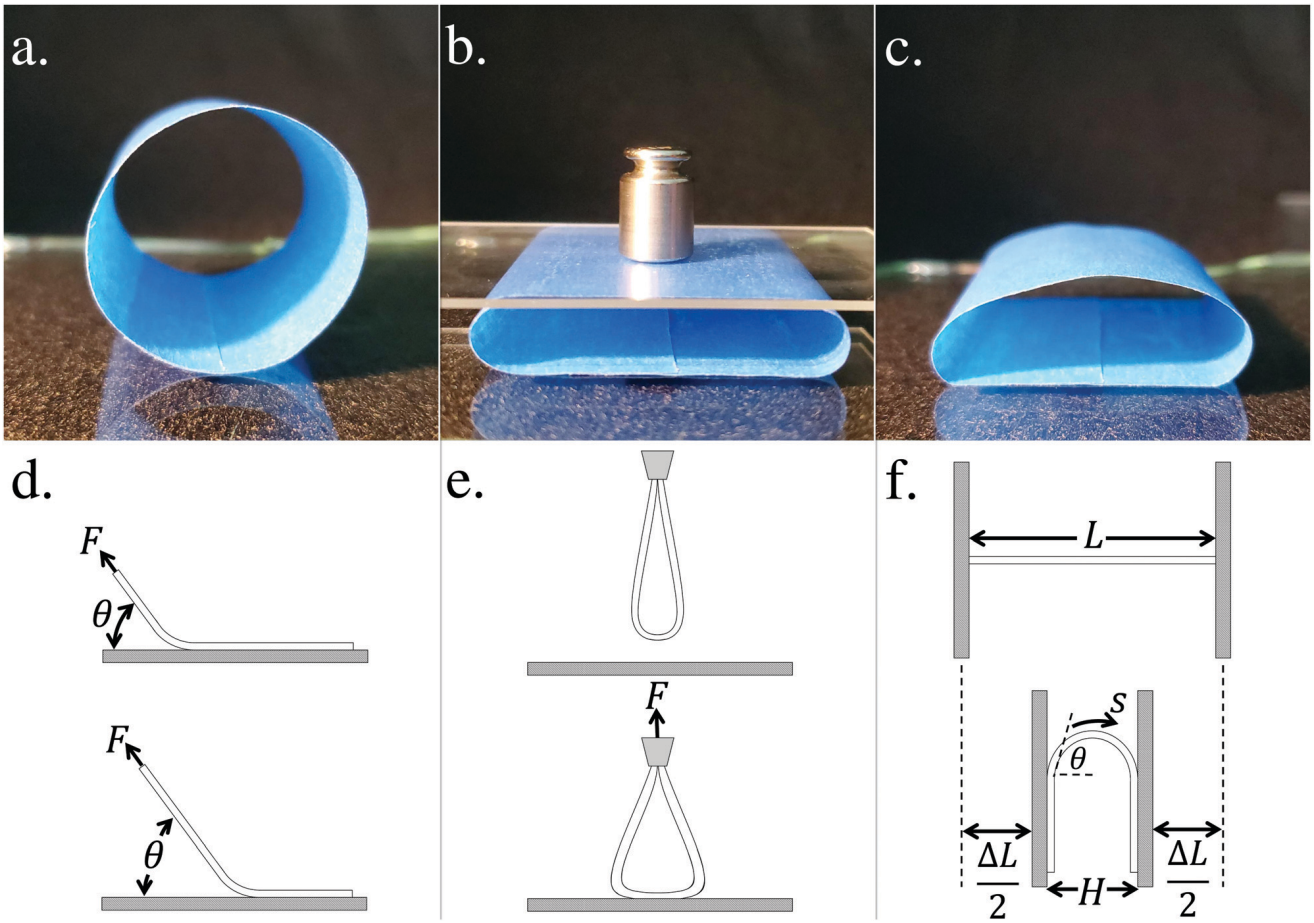

Fig. 1 Geometry of a tape loop. (a) A tape loop resting on a clean glass surface. (b) A compressed tape loop. (c) A tape loop after compression is removed. (d) Schematic of a peel experiment. (e) Schematic of a loop-tack test. (f) Schematic of the tape loop experiment discussed here.

wherein only a ruler is necessary to measure a system's adhesive properties.

The adhesion of a thin film to a flat substrate is typically described by peel mechanics, a very successful model that has developed over the past 50 years and is a staple in industrial adhesion testing.[1–5] To remove a thin piece of tape of width, b, from a substrate, a force, F, must be applied to the free end of the tape which is at some angle, θ, with respect to the substrate (see Fig. 1d). If the applied force is large enough, a crack between the tape and substrate will begin to propagate along the interface, destroying adhesive interface and creating new substrate/air and tape/air interfaces in the process. In the language of fracture mechanics, the energy release rate, $G = \partial U_M/\partial A$ is equal to the Dupré work of adhesion, $\Delta\gamma$, at this point. Here U_M is the stored mechanical energy of the system and A is the amount of contact between the film and substrate. Careful analysis, coupled with the assumptions of film inextensibility and neglecting bending, allows the critical force to peel the tape to be related to the work of adhesion as:

$$F = \frac{\Delta\gamma b}{1 - \cos(\theta)}. \quad (1)$$

Peel experiments are often performed at 90°, where eqn (1) becomes simply $F = \Delta\gamma b$. Over the years, many additional features have been added to the model (plasticity or stretching in the film, bending of the film, shear lag, friction, *etc.*), enabling the model to successfully describe almost any scenario involving the removal of a thin adhered sheet from a solid substrate by application of a force to one end.[4,6–12]

When a film is bent in a loop, the direct application of eqn (1) is no longer permitted because U_M will now depend on the film shape, which itself will change during an experiment. The loop-tack test is a good example of a common industrial thin-film adhesion test that involves film curvature.[13–19] In this case, a film is bent back on itself to form a 'tear-drop' shape, rather than a cylindrical loop (Fig. 1e). The sharp side of the tear-drop shape is clamped and the curved, free side of the film is then pushed into contact with a flat substrate and pulled off as forces are measured. Much effort has been made to model the test, but simple expressions of the type of eqn (1) do not currently exist. Interestingly, experiments have shown that the indentation part of the test cycle is independent of the system's work of adhesion.[16] Pull-off curves typically show a quick rise of force, a plateau and a final sharp peak force before ultimate separation of the film and substrate.

Recently, adhesion and the loop geometry have seen great interest due to the increasing use of nano-scale tubes such as carbon nanotubes in electronics.[20–32] Researchers have observed

that tubes of this scale will often show a deformed shape when placed on a flat substrate,[20–22] and a variety of models using techniques ranging from variational methods to molecular dynamics have been developed to describe the observations.[23–32] Models show a deposited tube will 'flow' to its equilibrium deformed shape in contrast with the macroscopic loop (though metastable states have been noted). This is not surprising as nanotubes are dominated by long range attractive and thermal forces which will overcome energetic barriers on the nano-scale in the same way as compression will on the macro-scale.

Below we describe the details of our experimental procedures before describing our modeling of the tape loop. We then show basic experimental results such as typical force–displacement curves and shapes of the free part of the loop at various stages in the experiment. We next discuss the force–displacement cycle in detail, before describing a version of the experiment which exploits the zero load limit as simple, physically grounded, adhesion measurement technique.

2 Experimental

Our experimental geometry is shown in Fig. 1f. The loop is simplified to a half-loop in order to avoid the complexities of joining sheet ends to form a true loop. For example, the effect of an overlap region which is of twice the film thickness, a distorted surface contact near the overlap, or residual stresses created during joining would all confound results. Because of the symmetry of the problem, and that we are not exploring the final stages of loop removal, our choice is not expected to alter the basic mechanics.

2.1 Sample preparation

Polydimethylsiloxane (PDMS) was made into films from a Sylgard 184 elastomer kit. Different weight ratios of prepolymer to crosslinker were prepared: 10 : 1, 20 : 1, 30 : 1, 40 : 1, 45 : 1, and 50 : 1. The elastomer base was thoroughly mixed with the curing agent *via* continual stirring for 10 min. The PDMS mixture was then poured into a polystyrene sample dish to a desired weight based on an anticipated thickness. Thinner samples were prepared by spin-coating PDMS on a polyacryilc acid release layer coated glass slide. The samples were then placed in vacuum oven at 25 in/Hg pressure and then pressure was released after five minutes. Cycling was repeated 4 times in order to evacuate all gas bubbles from the mixture. The samples were then heated to $\sim$85 °C for 90 minutes under 15 in/Hg vacuum. Samples were promptly removed after the 90 minute anneal and quick quenched on a cool surface for a minimum of 30 minutes before use.

Polycarbonate films (PC) were made from solutions of 1–2% PC pellets, MW 60 kg mol^{-1} (Scientific Polymer Products), dissolved in chloroform (Fisher Scientific, Optima grade). Nile Red dye was often mixed into solutions to aid in imaging. Solutions were spin-coated onto a freshly cleaved mica surface that was placed in a closed chamber. The closed chamber had excess chloroform, a volatile solvent which provided vapor pressure to slow evaporation. After a set time film was removed and annealed at $\sim$180 °C for several hours.

Samples were then cut into long rectangular strips of varied widths and floated off their substrates on the surface of Milli-Q water. The exact dimensions, length, width, and thickness of these strips were measured with calipers and/or image analysis. Next, each end of a strip was placed flush against one of the two parallel plates of our apparatus. The distance of the plates was adjusted to a distance where the section of film between the two plates assumed an approximately circular curvature. Care was taken to ensure bonding surfaces were not handled during the setup process.

2.2 Apparatus

The apparati used in these experiments are documented in a previous publication.[33] In brief, the apparati consisted of two parallel glass plates, one plate attached to a force sensor and the second plate attached to an actuator. A camera was positioned beside the plates in order to capture the vertical plate motion. Two different versions were constructed. The macro version used a Newport Motion Controller Model ESP 301 motor while the micro version used a PI N-381 nanopositioner. Additionally, the micro version was placed on an Olympus Flouview FV1000 laser scanning confocal microscope (LSCM) stage for 3-D imaging. 3-D imaging provided us a detailed shape of the film at each stage of compression.

An additional horizontal apparatus was also created, in order to quantify the film at a point of zero load. Similar to the previous set-up a film was bent and placed between two glass plates. However, in this case two films were placed

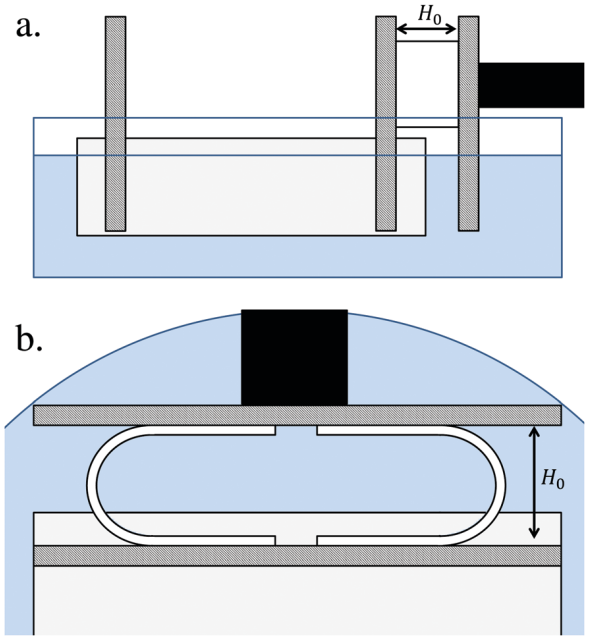

Fig. 2 A simplified adhesion measurement apparatus. (a) Shows a side view and (b) shows a top down view. Light grey is the 'boat', black represents a rigid connection to the table, blue shows water in a crystallization bowl and glass plates are shown as cross-hatched rectangles. Two bent films are shown in white.

symmetrically between the plates, forming two bends rather than one. One plate was fixed in position. In order to reduce friction the second plate was fixed to a ''boat''. The ''boat'' was created from a counterbalanced container constructed with a 3D printer and rests on a water surface (see Fig. 2). In this experiment the loops are compressed beyond the elastocapillary length by hand, and then allowed to relax to equilibrium.

3 Modeling

3.1 Scaling

We begin modeling with a terse scaling analysis. First, we identify the elasto-capillary length, $\ell_{ec} = \sqrt{B/\Delta\gamma}$ as the relevant system lengthscale. Here B is the bending modulus which is equal to $Eh^3/12(1-\nu^2)$ where E is the Young's modulus, h is the film thickness, and ν is the Poisson ratio. The system is expected to behave differently as the confining lengthscale becomes large or small compared to ℓ_{ec}.[34] In the present case, the confining length is the size of the gap between the two parallel plates, H, hence we expect two regimes of behaviour over the course of the experiment. Conjugate to H is the measured force, P, for which there is no, a priori, natural scale.

If $H > \ell_{ec}$ the system is unconfined, and bending should not be so important. If the film is inextensible, this means that the only way it can accommodate a change in H is to open along the interface by the same amount. When an amount of area is opened ($b\delta H$) a work ($F\delta H$) must be done. A simple energy balance then gives a tensile value of $F \sim \Delta\gamma b$, which is the 90° peel-test result. Note that there is no hint of the symmetry between opening and closing to be broken here.

On the other hand, as $H < \ell_{ec}$, confinement and bending become dominant. Here we expect an energetic balance between bending and work done, which leads to the well known 'adhesion free' bending result: $F = \pi Bb/H^2$, a compressive force.[33] Again, there is no opening/closing symmetry breaking apparent here either.

The two limits suggest that rescaling distances by ℓ_{ec} and forces by $\Delta\gamma b$ will lead to universal behaviour. If this is the case, scaling predicts the system to follow a single force–displacement curve which scales as H^{-2} at small H and asymptotically approaches a constant value of -1 at large H.

3.2 Sticky elastica

For a more complete picture of the process we consider the full system energy and aim to calculate both the shape of a loop and its force–displacement curve directly. To do so, we adapt the 'Sticky Elastica' model to the loop geometry, ignoring the scaled variables suggested above for clarity.[35] One of the key outcomes of this analysis is that the boundary conditions are not all unrelated to the material specific details of the surfaces.[35–38] Adhesion influences the curvature of the film at the point of attachment to the wall and the oft assumed zero-curvature boundary is proven incorrect for cases in which $\Delta\gamma \neq 0$.

Considering the geometry shown in Fig. 1f. Here $\theta(s)$ describes the angle with respect to horizontal made by an adhesive thin inextensible sheet and s is a coordinate that follows the contour of the sheet. The sheet, of length L and width b, makes contact with the parallel confining walls up to the point $\ell/2$ where it forms a free curve. The boundary conditions are thus $\theta(\ell/2) = -\pi/2$ and $\theta(-\ell/2) = \pi/2$. Alternatively, as the system is symmetric about the origin we could infer that $\theta(0) = 0$. The confining walls have been moved towards one another such that the gap has a width of $L - \Delta L$.

The total energy per sheet width is given by:

$$U = \int_{-\ell/2}^{\ell/2}\left[\frac{B}{2}(\theta')^2 + \Delta\gamma\right]\mathrm{d}s - L\Delta\gamma - \alpha\left(L - \Delta L - \int_{-\ell/2}^{\ell/2}\cos(\theta)\mathrm{d}s\right), \quad (2)$$

where θ' is $\mathrm{d}\theta/\mathrm{d}s$, and α is a Lagrange multiplier which physically corresponds to the load per unit width, P. An additional term could be added to ensure the vertical length constraint (*e.g.* $-\alpha_2\left(L - \Delta L - \int \sin\theta \mathrm{d}s\right)$) could be added to eqn (2). However, as we assume no shear force occurs at the contact point, the additional Lagrange multiplier goes to zero. We omit it for clarity. We also note our inclusion of the term $-L\Delta\gamma$ which is necessary to account for the contact energy scaling with the total film size L. While important to the total energy, we note this term does not affect forces or the shape of the film and could be neglected for convenience. Before minimizing, it is helpful to exploit symmetry:

$$U = 2\int_{0}^{\ell/2}\left[\frac{B}{2}(\theta')^2 + \Delta\gamma\right]\mathrm{d}s - L\Delta\gamma - \alpha\left(L - \Delta L - \int_{0}^{l/2}\cos(\theta)\mathrm{d}s\right). \quad (3)$$

Eqn (3) can be minimized in order to identify the minimal curve, $\theta(s)$, however, as pointed out by Wagner and Vella, both ℓ and α may also change, hence variations of all three quantities must be simultaneously considered.[35] We use an alternative calculation which arrives at the same result ESI:†

$$\theta'' = -(\alpha/B)\sin(\theta). \quad (4)$$

Again we note that $\alpha = P$, and we make this substitution in all following steps. The length constraint is unchanged:

$$L - \Delta L = 2\int_{0}^{\frac{\ell}{2}}\cos(\theta)\mathrm{d}s, \quad (5)$$

and finally a new additional constraint emerges:

$$\theta'(\ell/2) = \sqrt{(2\Delta\gamma)/B} = (\sqrt{2}/\ell_{ec}). \quad (6)$$

Note that were it not for this natural boundary condition, our results would be identical to the rectangular elastica, which has been much studied.[39–42] This is also the case for the $\Delta\gamma \to 0$ limit.

3.3 Solutions

Eqn (4) can be solved analytically using an elliptic integral of the first kind. Integrating once gives an expression for the

curvature:

$$\theta' = \sqrt{2(P/B)\cos(\theta) + c_1}, \tag{7}$$

where c_1 is an integration constant. If eqn (6) is to be accommodated, then c_1 must be equal to $(2\Delta\gamma)/B$. Solving the differential equation yields:

$$\theta(s) = 2am\left(\sqrt{\frac{P+\Delta\gamma}{2B}}s,\ \sqrt{\frac{2}{1+\Delta\gamma/P}}\right), \tag{8}$$

where am is the Jacobi amplitude function. The point of contact, ℓ, can also be explicitly determined:

$$\frac{\ell}{2} = F\left(-\frac{\pi}{4}, \sqrt{\frac{2}{1+\Delta\gamma/P}}\right)\sqrt{\frac{2B}{P+\Delta\gamma}}, \tag{9}$$

where F is the eliptic integral of the first kind. We note that we have recovered the result of Majidi.[38]

If $P = 0$, eqn (4) can be integrated twice, yielding $\theta(s) = a_1 s + a_2$. Given the boundary condition for θ at $s = 0$ and $s = \ell/2$ we can further determine that $a_2 = 0$, and $a_1 = -\pi/\ell$. The curve is fully specified if the curvature, a_1, can be uniquely defined (requiring an additional boundary condition). Eqn (6) would solve this problem, however, this boundary condition can only be satisfied at a single point (when $H = \sqrt{2}\ell_{ec}$). We discuss this point in greater detail in Section 4.5 below.

4 Results and discussion

4.1 Basic experimental results

The raw experimental results are shown in Fig. 3 and 4. The former shows a typical force–displacement curve and the latter shows the shape of the free-standing part of the film at various stages of the experiment. Starting at the point labelled 1. on the force curve, the two walls increasingly confine the PDMS film up to some arbitrarily chosen peak compression. This segment of the cycle begins with a near zero force which is always positive and monotonically increases during compression. Regardless the magnitude of the adhesive force (this varies with the mixing ratio for PDMS), the curve is quantitatively

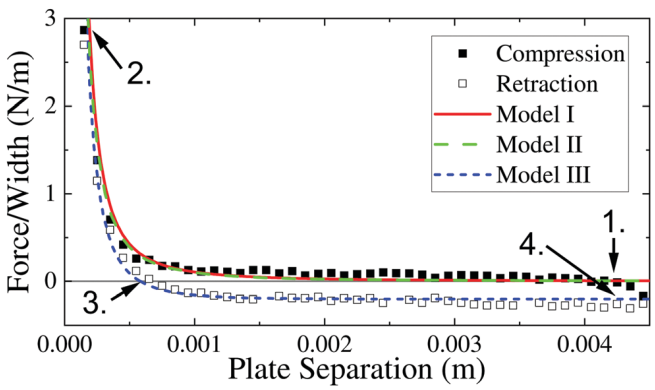

Fig. 3 A typical force displacement curve for a 10 : 1, thickness 56.4 μm film. Fits to the circular, Rectangular Elastica and Sticky Elastica model are shown.

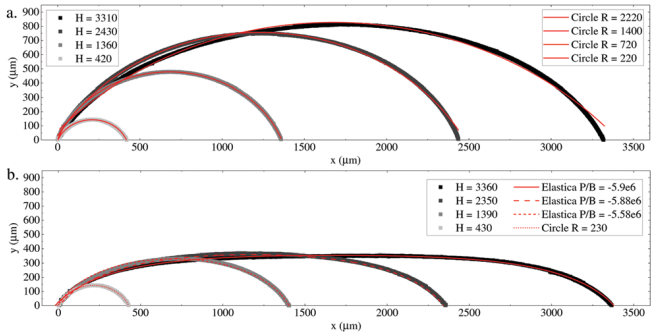

Fig. 4 Film shapes measured by confocal microscopy at various stages of compression (a) or retraction (b). (a) Shows circular fits (solid red curves, radii of 2220, 1400, 720, 220 respectively) as well as fits to the Rectangular Elastica. Disagreement between the Rectangular Elastica and the measured film is more pronounced for the wider separations, suggesting gravity may play a role. (b) Shows the same film during retraction and fits to the equilibrium "Sticky Elastica" model. Physically measured plate separations are shown in the caption for both compression and retraction, and fits are truncated at the apparent contact point ($y = 0$).

consistent with earlier predictions for adhesion-free elastic films.[33] This can also be verified by experimentally removing any adhesion by coating PDMS films with a monolayer of cornstarch particles. Films at all points between 1. and 2. maintain shapes that are well described as cylindrical, again in agreement with adhesion free films (circular fits are shown in Fig. 4a). While the true shape in this region may not be circular, we emphasize that the shape must be so nearly circular that there is effectively no difference.

After peak compression (point 2.), the sample walls are moved apart and forces are observed to drop more quickly than they rose on approach. Notably, the force drops to zero well before the confining walls have reached their initial separation. The sample's shape at point 3. is also very well described as cylindrical.

Further plate separation drives forces below zero and the sample moves into a tensile rather than compressive regime (points 3. to 4.). At large separations, the force approaches a constant value. At large separation, one would expect the test to be identical to a 90° peel test, thus eqn (1) can be used to determine a critical energy release rate. In the case of the film shown in Fig. 3 the energy release rate is found to be $G_c = 0.27 \pm 0.02$ N m^{-1} when the motor is moving the plates at a quasi-static (average) rate of $1 \times 10^{-5} \pm 2 \times 10^{-6}$ m s^{-1}, but with the motor moving incrementally at a rate of 3×10^{-3} m s^{-1}. This value is consistent with published measurements using a more conventional glass sphere indentation test (a JKR adhesion test).[43,44]

This cycle is repeatable; when the motor is reversed to compress the sample again the same curve is traced. Likewise, the same shapes are observed with each repeated loop. The hysteresis observed does not have to do with loose film due to improper film placement or other transient issues. Wait times at different stages of the test also do not heavily influence the curves. For example, waiting at point 1. has no effect. Waiting at point 2. a small logarithmic relaxation is noted and has previously been attributed to material (not adhesive) processes.[33]

Finally, we note that although hysteresis is not uncommon in adhesion measurements what is observed here is atypical.[45–48] For example in measurements between a PDMS sphere and a PDMS flat it is typical to record an energy release rate of 20 mN m^{-1} while advancing contact and a value of 100 mN m^{-1} or more when receding. What is different here is that the advancing curves measure an adhesion value of zero during advance (rather than just a smaller value). Were there to be some adhesion, the advancing curve would have to be negative at large separations and pass through zero at some fixed plate separation (see discussion of this point below).

4.2 Indentation analysis

The indentation segment of the force–displacement curve (region 1. to 2.) appears insensitive to the work of adhesion. Fig. 3 shows a fit to the zero adhesion model described in ref. 33 (Model I). The model assumes a circular cross-section for the free part of the film and balances bending with work as described in Section 3.1. The only free parameter in the fit is the Young's modulus of the film, and the fit value precisely matches the modulus measured by more conventional means.

The elastica model can also be used to fit this region, under the same assumption that the work of adhesion is zero and with the additional assumption that the Lagrange multiplier, α, is equal to the applied load (Fig. 3, Model II). Shapes generated are the well-known Rectangular Elastica and although not circular are near circular away from the bounding walls (see Fig. 4). Given the measured force and measured wall separation the shape of the elastica does not closely match the measurement. Experiments may not resolve the true contact points of the films, and it is likely for the large separations (where the discrepancy is largest) that gravity contributes to the film shape.

More importantly, that $\Delta\gamma$ is zero upon approach but non-zero upon retraction is simply unphysical. $\Delta\gamma$ is a measure of surface energies, and is a fixed materials property of the system. It simply cannot disappear due to the direction of motion. This is a key point we wish to raise in this article, and its resolution we believe has to do with the oft ignored aspects of stability which enter many adhesion problems.

To more clearly address this anomaly, let us consider adhesion as a fracture process. In this case, propagation of an interfacial crack is determined by comparison of the work of adhesion with the system's energy release rate:

$$G = \frac{\partial U_{\mathrm{M}}}{\partial A}, \tag{10}$$

where U_{M} is the mechanical energy of the system and A is the area opened by the propagation of a virtual crack. The energy cost to move the crack a 'virtual' distance is then given as:

$$\partial U = (G - \Delta\gamma)\partial A. \tag{11}$$

If $G > \Delta\gamma$ the crack will only reduce the overall energy if it decreases in area (opens), if $G < \Delta\gamma$ then the energy is decreased by closing the crack (∂A increases). The system is in equilibrium only if $G = \Delta\gamma$.

In general the energy release rate is what is measured in an experiment, not the work of adhesion. This is because the system is not necessarily in equilibrium at each step, which will happen if the crack moves more slowly than the instrument. We specifically use this language to emphasize that we are measuring an energy release rate below.

The crack can only grow or shrink if it is unstable at the particular plate separation in question. This could be determined by taking an areal derivative of G. If $\partial G/\partial A > 0$ the crack is stable and can only open or close if the plates are moved. Importantly, if $G < \Delta\gamma$ and $\partial G/\partial A > 0$ a crack could be 'stuck' in a non-equilibrium state. The system would be frustrated as appears to be the case observed here. As is commonly the case with frustrated systems, the system is history dependent. In this case, compression causes the free length of the loop (ℓ) to be fixed (as the crack cannot move until the walls move) and the local problem becomes simply minimizing the bending energy. The film adopts the smallest curvature which fits between the walls – a Rectangular Elastica.[41]

Consider the process taking place in two steps, a common conceptual exercise in adhesion problems.[3] First a purely elastic deformation is caused by the plate boundaries (ignoring adhesion). Next, adhesion is 'turned on' and the interface adjusts to a new equilibrium. In the case of the loop, the second step amounts to the curvature at the contact point becoming non-zero in accordance with the adhesive boundary condition derived above. This cannot happen without the contact point moving along the interface, something that could not happen if the crack is stable ($\partial G/\partial A > 0$).

4.3 Retraction analysis

When the plates are opened again (for example, point 2. to point 3. and 4. in Fig. 3) the interfacial crack remains fixed in place as the plates open. Opening leads to a reduction in curvature in the film, but the film does not follow the 1. and 2. path. Instead, the system adjusts the boundary conditions at the contact point, and θ' increases from zero. At some point the increase stalls $\left(\theta' = \sqrt{2\Delta\gamma/B}\right)$ and the interface must open as the plates move, following the true equilibrium curve discussed above. Results of the equilibrium are shown as the dashed curve (Model III) in Fig. 3. Shapes predicted by the model are extremely accurate in this regime as can be seen in Fig. 4.

There are an infinite family of curves which an experiment might follow, depending on when compression is stopped and the motor is reversed. However curves are always bound by the "$\theta' = 0$" curve above and the "Sticky Elastica" curve below. Interestingly, provided the system is compressed beyond the elastocapillary length, the force displacement curve will always pass through the unique point $H_0 = \sqrt{2B/\Delta\gamma}$ as $P = 0$. We discuss the implications of this unique point below.

4.4 Modulus and energy release rate measurement

Experiments were repeated with PDMS samples of different thicknesses, dimensions and cross-linking ratios. The tape loop geometry allows fitting the indentation curve to yield a

measurement of the bending modulus, something not easily possible in either a loop-tack or peel test. Independently measured thickness values allow the Young's modulus to be determined, which we plot in Fig. 5a. As is widely acknowledged, higher ratios lead to lower modulus materials.[49–55]

More interestingly, higher ratios also lead to larger measured values of the energy release rate (G_c). The increase is likely due to increased viscoelasticity at the interface in the softer materials. Fig. 5b provides a summary of our measurements. Though measurements of adhesion with PDMS have been done for quite some time, we believe this to be the first quantitative measurement of G_c between PDMS and glass for this wide range of cross-linker ratios.[44,45,51,54,56–63]

As a convenience for prediction of the energy release rate for mixtures not directly measured here, we plot the correlation of G_c with moduli in Fig. 6. We find the data is well fit by $G_c = AE^{-n}$ where $A = 200 \pm 60$ and $n = 0.49 \pm 0.03$. We caution that this is an entirely empirical fit; there is no reason to believe a power law is the correct form of the relationship and the rule is likely error prone beyond the measured range of Fig. 6. Furthermore, the modulus of Sylgard 184 is not only cross-linker ratio dependent but is also highly related to annealing temperature. It is unclear if changes in annealing temperature affect measured G_c differently than its modulus alone would suggest.

Experiments were also conducted with very thin ($\sim$2 μm) polycarbonate films. Polycarbonate is a glassy polymer at room temperature and is therefore expected to suffer very little viscoelastic loss during an experiment. Similar behaviour was noted (hysteresis in force–displacement curves, no adhesion sensitivity on indentation, negative forces during retraction), verifying our contention that the hysteresis is not due to viscous loss. We measured moduli of 1.6 ± 0.01 GPa and energy release rates of 0.04 ± 0.05 N m^{-1}. The high error in energy release rate we believe is due to significant static charge present in the system. Even neutralization with a Zerostat 3 and long wait times after a sample was loaded the parallel plate setup did not result in highly repeatable values. We therefore do not believe our measurement is an accurate measurement of true polycarbonate/glass interfaces, but is convoluted with some amount of electrostatic adhesion.

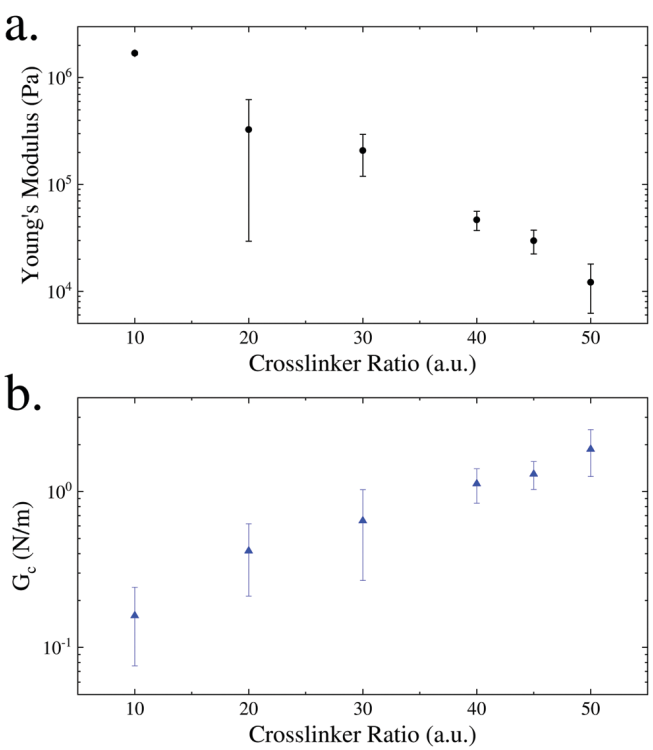

Fig. 5 (a) Young's modulus as a function of crosslinker ratio (arbirary units) as measured from indentation curves. Error bars denote the standard deviation of the measurements. (b) Energy release rate as a function of crosslinker ratio.

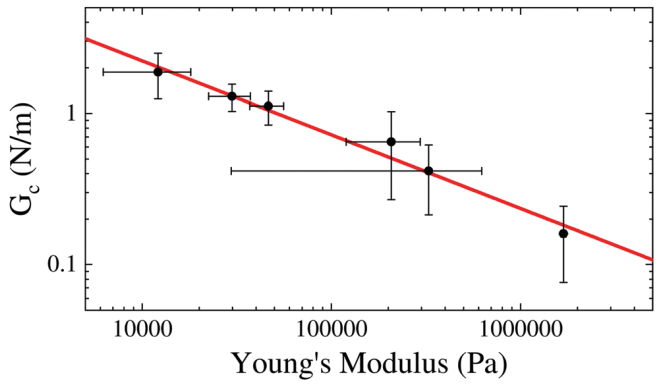

Fig. 6 Data from Fig. 5(a) and (b) plotted G_c *vs.* Young's Modulus. A power law fit is shown by the solid curve.

Finally, we would like to point out the versatility and simplicity of the technique and compare with other accepted technologies. First, all that is necessary to do a tape-loop measurement is a force transducer sensitive enough to measure $2\Delta\gamma/b$, where b is the film width which can easily be adjusted to fit a given transducer. Given that a force transducer can be constructed from any cantilever, the method is somewhat unlimited in sensitivity. We do point out that material failure would limit peak forces measurable here. Compared to a loop-tack test, the tape loop has a relatively simple theoretical framework (and very simple limits) and no issues of out of plane bending. The tape loop requires much less total length than would be safe for a typical peel setup and as no direct visual observation is necessary, the technique could be scaled to nano-scale materials. Provided no material changes occur during a cycle, experiments can be repeated indefinitely to increase sensitivity. And lastly, the technique does not rely on soft materials or casting a material in a mould as would a JKR experiment.[47] Alternatively, a thin film may be laid over a soft spherical JKR probe, but given the problem of wrapping a sphere with a flat sheet it is likely that such an experiment would cause an unclear stretching state for the film in question, which might influence adhesion measurements in unknown ways.

4.5 A simple technique for the measurement of energy release rates

Once a loop is compressed beyond the capillary length and the load is reduced to zero, the loop will follow the equilibrium

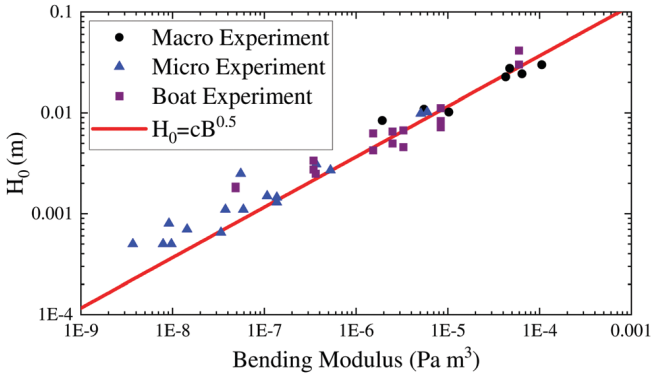

Fig. 7 Data validating the simple adhesion measurement. H_0, the plate separation at $P = 0$, is plotted against the bending modulus for various 10 : 1 PDMS films. Data from both macro and micro setups as well as the 'boat' experiments all fall along a common square-root curve as discussed in the text.

curve described by eqn (8). At the point of zero load, the loop forms a stable structure with a well defined plate separation. Noting that $am(u,m \to 0) \to u$ the shape of the free portion of film becomes exactly circular as eqn (8) reduces to $\theta(s) \to \sqrt{2}s/\ell_{ec}$. Hence, the plate separation is given by:

$$H_0 = \sqrt{2}\ell_{ec} = \sqrt{\frac{2B}{\Delta\gamma}} \tag{12}$$

It is notable that the plate separation at this point relates only to two material properties – the bending modulus and the energy release rate (work of adhesion). Simply, this means that if a loop's modulus is known the separation can give a direct measurement of the systems adhesive properties. We demonstrate this observation in two ways.

First, for all the PDMS experiments run, we can extract and plot the plate separation as a function of bending modulus (see Fig. 7 where we show only 10 : 1 PDMS for clarity). For both micro and macro experiments, we see this data falls along a slope of $\sim$0.5 on a log–log axis (eqn (12)).

Secondly, we constructed a frictionless horizontal setup by creating a floating "boat" which held one parallel plate next to a "wall" holding the second parallel plate. Between the two parallel plates two opposite facing half loops were arranged (two are now necessary to balance moments). The floating side was then pushed by hand towards the fixed plate. When the distance between the two parallel plates was smaller than the estimated elastocapillary length, pressure was removed and the system was allowed to relax. After waiting times ranging from 30 min to 12 h the plate separation was measured through image analysis and a cell phone camera. With the measured modulus of 10 : 1 PDMS and the film thickness, this data was also added to Fig. 7.

The data from all three experiments falls along the same trend and is well fit by a square root relation ($H_0 = cB^{0.5}$). The fit's only free parameter, the power law amplitude c yields a value of 3.67 $\pm$ 0.14 though the fitting error likely under estimates the true variation. The result is a measurement of $\Delta\gamma = 0.15 \pm 0.006$, which is in fair agreement with the average value measured by direct fitting of the full sticky Elastica model and published values.[43,44]

5 Conclusion

In this work we have outlined how the Sticky Elastica model can be adapted to the tape-loop geometry and used to fit experimental data. We show that force–displacement loop hysteresis is due to crack stability, rather than a direction dependent work of adhesion. The loop geometry is seen to provide a reliable and simple method to measure both film modulus and energy release rates, which we demonstrate with a suite of polydimethylsiloxane elastomers as well as polycarbonate films. Finally, the model suggests using the point of zero load in a force–displacement cycle as a force sensor free method of adhesion measurement.

Conflicts of interest

There are no conflicts to declare.

Acknowledgements

ABC would like to acknowledge helpful conversations with James Hanna and Marcelo Diaz. TE would like to thank the support of the NDSU Materials and Nanotechnology Program. HS acknowledges support by Swiss National Science Foundation grant 200020182184 to J. H. Maddocks. ABC acknowledges support from the National Science Foundation under Grant No. CMMI-2011681.

References

1 D. H. Kaelble, *Trans. Soc. Rheol.*, 1959, **3**, 161–180.
2 K. Kendall, *J. Adhes.*, 1973, **5**, 179–202.
3 D. Maugis and M. Barquins, *J. Phys. D: Appl. Phys.*, 1978, **11**, 1989–2023.
4 M. D. Thouless and H. M. Jensen, *J. Adhes.*, 1992, **38**, 185–197.
5 ASTM Standard D903 - 98(2017), Standard Test Method for Peel or Stripping Strength of Adhesive Bonds, ASTM International, West Conshohocken, PA, 2017.
6 K. Kendall, *J. Phys. D: Appl. Phys.*, 1975, **8**, 1449–1452.
7 A. N. Gent and G. R. Hamed, *J. Appl. Polym. Sci.*, 1977, **21**, 2817–2831.
8 K.-S. Kim and N. Aravas, *Int. J. Solids Struct.*, 1988, **24**, 417–435.
9 Z. Peng and S. Chen, *Phys. Rev. E: Stat., Nonlinear, Soft Matter Phys.*, 2015, **91**, 042401.
10 A. Ghatak, L. Mahadevan and M. K. Chaudhury, *Langmuir*, 2005, **21**, 1277–1281.
11 S. Ponce, J. Bico and B. Roman, *Soft Matter*, 2015, **11**, 9281–9290.
12 M. Thouless and Q. Yang, *Int. J. Adhes. Adhes.*, 2008, **28**, 176–184.

13 R. H. Plaut, N. L. Williams and D. A. Dillard, *J. Adhes.*, 2001, **76**, 37–53.
14 R. H. Plaut, A. J. Dalrymple and D. A. Dillard, *J. Adhes. Sci. Technol.*, 2001, **15**, 565–581.
15 Y. Woo, R. H. Plaut, D. A. Dillard and S. L. Coulthard, *J. Adhes.*, 2004, **80**, 203–221.
16 J. Qi, D. A. Dillard, R. H. Plaut and J. G. Dillard, *J. Adhes.*, 2003, **79**, 559–579.
17 ASTM Standard D6195 - 03(2019), Standard Test Methods for Loop Tack, ASTM International, West Conshohocken, PA, 2019.
18 A. Srivastava and C.-Y. Hui, *Proc. R. Soc. London, Ser. A*, 2013, **469**, 20130425.
19 A. Srivastava and C.-Y. Hui, *Proc. R. Soc. London, Ser. A*, 2014, **470**, 20140528.
20 R. S. Ruoff, J. Tersoff, D. C. Lorents, S. Subramoney and B. Chan, *Nature*, 1993, **364**, 514–516.
21 N. G. Chopra, L. X. Benedict, V. H. Crespi, M. L. Cohen, S. G. Louie and A. Zettl, *Nature*, 1995, **377**, 135–138.
22 T. Hertel, R. E. Walkup and P. Avouris, *Phys. Rev. B: Condens. Matter Mater. Phys.*, 1998, **58**, 13870–13873.
23 A. Pantano, D. M. Parks and M. C. Boyce, *J. Mech. Phys. Solids*, 2004, **52**, 789–821.
24 K. Yan, Q. Xue, Q. Zheng, D. Xia, H. Chen and J. Xie, *J. Phys. Chem. C*, 2009, **113**, 3120–3126.
25 J. Shi, S. Müftü and K.-T. Wan, *J. Appl. Mech.*, 2012, **79**, 041015.
26 J. Shi, S. Müftü, A. Gu and K.-T. Wan, *J. Appl. Mech.*, 2013, **80**, 061007.
27 X. Yuan and Y. Wang, *Int. J. Solids Struct.*, 2018, **144–145**, 144–159.
28 X. Yuan and Y. Wang, *Nanotechnology*, 2018, **29**, 075705.
29 X. Yuan and Y. Wang, *Soft Matter*, 2020, **16**, 1011–1020.
30 X. Yuan and Y. Wang, *J. Appl. Phys.*, 2018, **124**, 155306.
31 X. Yuan and Y. Wang, *J. Phys. D: Appl. Phys.*, 2017, **50**, 395303.
32 M. Li, H. Li, F. Li and Z. Kang, *J. Appl. Mech.*, 2018, **86**, 011013.
33 T. Elder, D. Rozairo and A. B. Croll, *Macromolecules*, 2019, **52**, 690–699.
34 J. Bico, E. Reyssat and B. Roman, *Annu. Rev. Fluid Mech.*, 2018, **50**, 629–659.
35 T. J. W. Wagner and D. Vella, *Soft Matter*, 2013, **9**, 1025–1030.
36 J. Obreimoff, *Proc. R. Soc. London, Ser. A*, 1930, **127**, 290–297.
37 N. J. Glassmaker and C. Y. Hui, *J. Appl. Phys.*, 2004, **96**, 3429–3434.
38 C. Majidi, *Mech. Res. Commun.*, 2007, **34**, 85–90.
39 R. Levien, The elastica: A mathematical history, Eecs department, university of california, berkeley technical report, 2008.
40 C.-Y. Wang, *J. Appl. Mech.*, 1987, **54**, 159–164.
41 C.-Y. Wang, *J. Appl. Mech.*, 1981, **48**, 199–200.
42 M. Diaz, Private Communication, 2019.
43 G. Miquelard-Garnier, A. B. Croll, C. S. Davis and A. J. Crosby, *Soft Matter*, 2010, **6**, 5789–5794.
44 Z. Li, H. Yu and Q. J. Wang, *Tribol. Lett.*, 2013, **49**, 291–299.
45 P. Silberzan, S. Perutz, E. J. Kramer and M. K. Chaudhury, *Langmuir*, 1994, **10**, 2466–2470.
46 C.-Y. Hui and R. Long, *J. Adhes.*, 2012, **88**, 70–85.
47 K. Shull, *Mater. Sci. Eng., R*, 2002, **36**, 1–45.
48 K. Kendall, *J. Adhes.*, 1975, **7**, 55–72.
49 J. D. Glover, C. E. McLaughlin, M. K. McFarland and J. T. Pham, *J. Polym. Sci.*, 2020, **58**, 343–351.
50 F. Schneider, T. Fellner, J. Wilde and U. Wallrabe, *J. Micromech. Microeng.*, 2008, **18**, 065008.
51 F. Carrillo, S. Gupta, M. Balooch, S. J. Marshall, G. W. Marshall, L. Pruitt and C. M. Puttlitz, *J. Mater. Res.*, 2005, **20**, 2820–2830.
52 T. K. Kim, J. K. Kim and O. C. Jeong, *Microelectron. Eng.*, 2011, **88**, 1982–1985.
53 I. D. Johnston, D. K. McCluskey, C. K. L. Tan and M. C. Tracey, *J. Micromech. Microeng.*, 2014, **24**, 035017.
54 S. Vlassov, S. Oras, M. Antsov, I. Sosnin, B. Polyakov, A. Shutka, M. Y. Krauchanka and L. Dorogin, *Rev. Adv. Mater. Sci.*, 2018, **56**, 62–78.
55 W. Lee, K. Yeo, A. Andriyana, Y. Shee and F. M. Adikan, *Mater. Des.*, 2016, **96**, 470–475.
56 M. K. Chaudhury and G. M. Whitesides, *Langmuir*, 1991, **7**, 1013–1025.
57 S. Perutz, E. Kramer, J. Baney, C.-Y. Hui and C. Cohen, *J. Polym. Sci., Part B: Polym. Phys.*, 1998, **36**, 2129–2139.
58 A. Galliano, S. Bistac and J. Schultz, *J. Colloid Interface Sci.*, 2003, **265**, 372–379.
59 Y. Cao, D. Yang and W. Soboyejoy, *J. Mater. Res.*, 2005, **20**, 2004–2011.
60 E. Kroner, R. Maboudian and E. Arzt, *Adv. Eng. Mater.*, 2010, **12**, 398–404.
61 E. Kroner, D. R. Paretkar, R. M. McMeeking and E. Arzt, *J. Adhes.*, 2011, **87**, 447–465.
62 J. Nase, O. Ramos, C. Creton and A. Lindner, *Eur. Phys. J. E*, 2013, **36**, 103.
63 Y. Yu, D. Sanchez and N. Lu, *J. Mater. Res.*, 2015, **30**, 2702–2712.

Electronic Supplementary Information for "Adhesion of a Tape Loop"

Theresa Elder

Materials and Nanotechnology, North Dakota State University, Fargo, USA.

Timothy Twohig

Department of Physics, North Dakota State University, Fargo, USA.

Harmeet Singh

Institute of Mathematics, École Polytechnique Fédérale de Lausanne, Lausanne, Switzerland.

Andrew B. Croll

Department of Physics, North Dakota State University, Fargo, USA. and Materials and Nanotechnology, North Dakota State University, Fargo, USA.

(Dated: August 20, 2020)

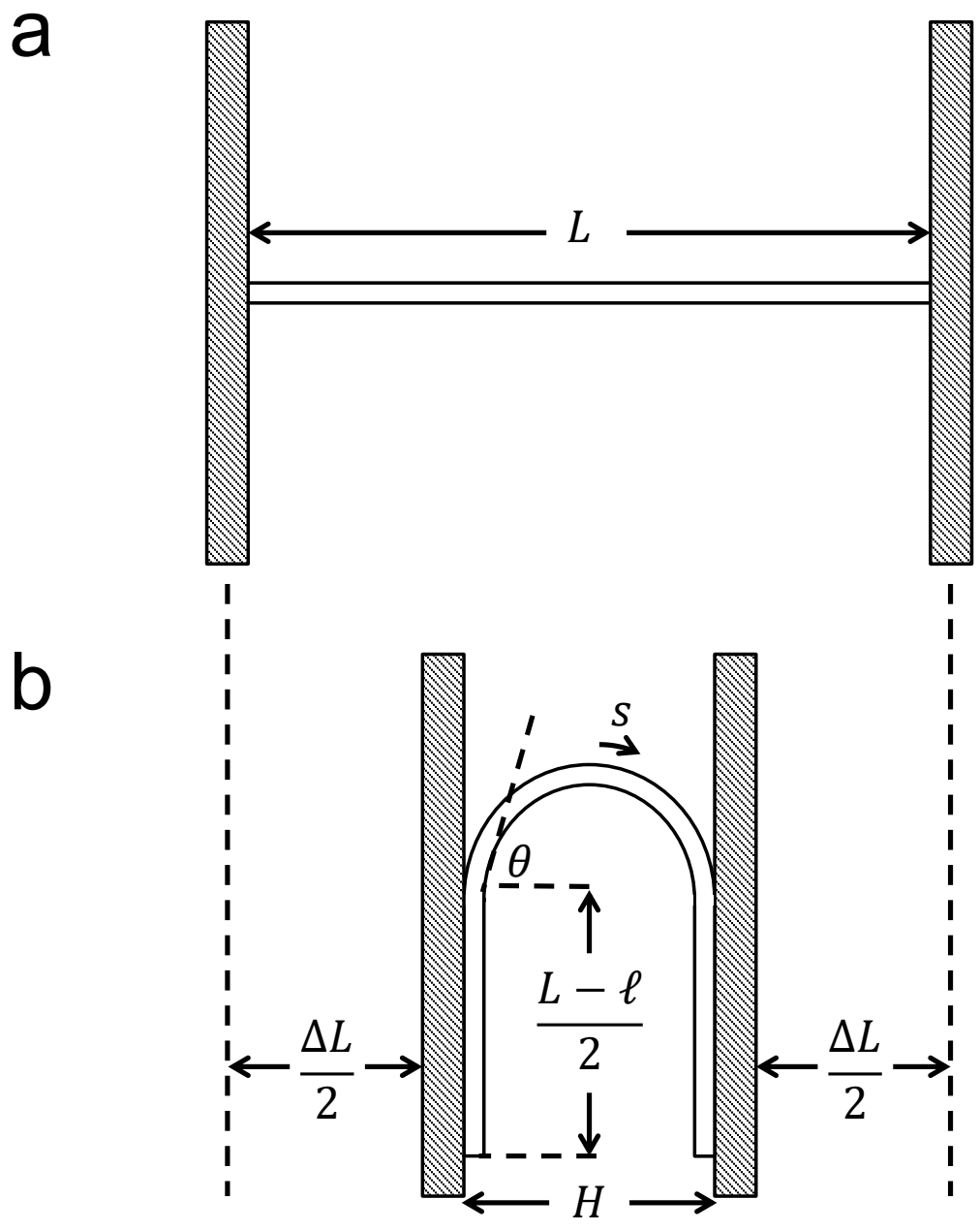

FIG. 1. Geometry of a tape loop. a. before compression of the walls, the film of length L lies flat. b. shows the film after some compression of the walls.

I. SURFACE ENERGIES

The net change in surface energy upon compression of a thin film between two walls can be determined by considering the total surface energy before and after a deformation.

Figure 1 shows the film before (a) and after (b) deformation. Initially the total of the interfacial energy is given by:

$$U_0 = 2L\gamma_{sa} + 2L'\gamma_{wa}, \tag{1}$$

where the sheet length is L, the wall length is L', and the subscripts s, w, a refer to sheet, wall, and air respectively. After compression some amount of sheet/wall contact is created, which comes at a cost γ_{sw}. If a length ℓ of sheet remains free from wall contact after compression, the total energy is given as:

$$U_1 = (L + \ell)\gamma_{sa} + 2(L' - (L - \ell)/2)\gamma_{wa} + (L - \ell)\gamma_{sw}. \tag{2}$$

The difference in energy is

$$\begin{aligned} U_1 - U_0 =& (\ell - L)\gamma_{sa} + (\ell - L)\gamma_{wa} - (\ell - L)\gamma_{sw} \\ U_1 - U_0 =& (\ell - L)(\gamma_{sa} + \gamma_{wa} - \gamma_{sw}) \\ =& (\ell - L)\Delta\gamma \end{aligned} \tag{3}$$

To ensure interfacial energy is reduced upon compression, $\Delta\gamma$ must be positive.

II. T-PEEL TEST

The sticky elastica variation shown in figure 1b is a variant of a geometry known in the literature as the T-Peel test.[1, 2] In a T-Peel test, the geometry shown in Figure 2, a load per unit width of film, P, is applied to the free end of two sheets which have been adhered to one another ($P = F/b$, F the applied force and b the out of page dimension in Fig. 2). As the sheets are pulled apart, they reach a steady state geometry and meet at an angle of 90° (assuming identical sheets). Analysis of the test is simplified by noting that the geometry reduces to two simultaneous 90° peel tests. In a peel test the energy release rate, G_c, is given by:

$$G_c = P(1 - \cos\theta), \tag{4}$$

where b is the film's width, θ is the angle between the film and the substrate and the film has been assumed to be inextensible.[3, 4] The relation arises through the geometry relating the work done by moving the load a distance (say dx) to the distance moved by the crack at the interface (say dc). In 90° peel $dx = dc$ if the film is inextensible.

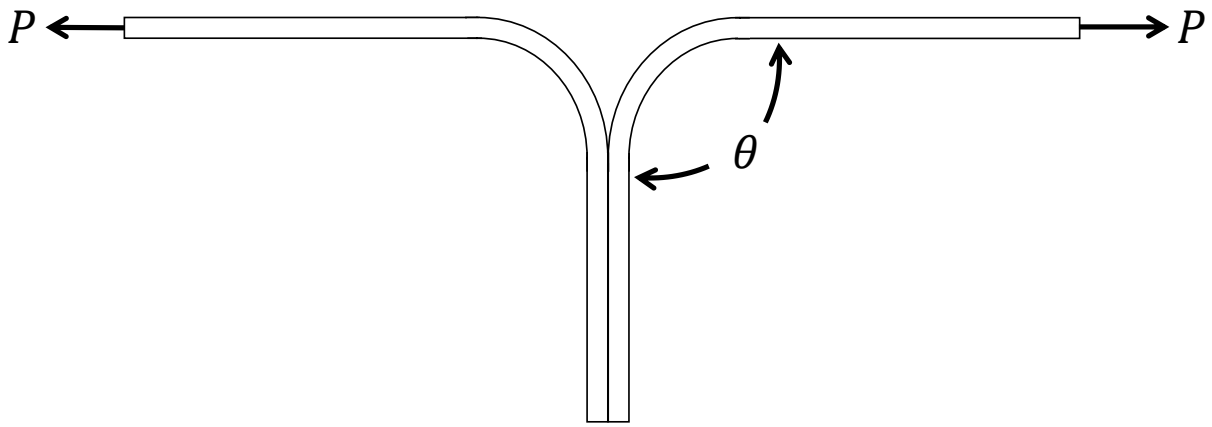

FIG. 2. Geometry of a T-Peel test.

What changes in the T-peel geometry is that the load at two positions must move a distance dx in order to open the same distance of crack, dc. The energy release rate in a T-Peel test is therefore only slightly different:

$$G_c = 2P. \tag{5}$$

III. STICKY ELASTICA

In this section, we adapt the "Sticky Elastica" model of Wagner and Vella [5] to the geometry shown in Figure 1 (a), and derive the governing equation and boundary condition applicable to our system.

We consider a configuration, as shown in Figure 1 (b), where a thin inextensible sheet of total length L and width b is compressed by moving the confining walls closer by a total distance ΔL. The angle made by the tangent of the sheet at any given arc-length coordinate s with the horizontal is denoted by $\theta(s)$. The two end points of the free part of the sheet where it contacts the confining plates are given by $s = \pm l/2$, and the entire configuration is assumed to be symmetric under reflection in a plane parallel to the confining walls and passing through the mid point of the sheet at $s = 0$. Exploiting this symmetry of the system,

we consider the following functional comprising the total energy of one symmetric half of the free part of the sheet, and the inextensibility constraint enforced by a constant Lagrange multiplier α,

$$U = \int_0^{l/2} ds \left[\frac{1}{2} B\theta'^2 + \Delta\gamma\right] - \alpha \left(\frac{L - \Delta L}{2} - \int_0^{l/2} ds \cos\theta\right) , \tag{6}$$

Here B is the bending rigidity of the sheet, and the prime represent the total derivative w.r.t. the arc-length parameter s, i.e. $()' \equiv \frac{d}{ds}$. The first term in the first integral above represents the bending energy density of the sheet, and the second term represents the adhesive penalty per unit length due to peeling. The constant α is a Lagrange multiplier enforcing the inextensibility constraint on the sheet. The boundary conditions are $\theta(0) = 0$ and $\theta(l/2) = -\pi/2$. We also note, that for clarity in the derivation we opt to absorb the constant term $-L\Delta\gamma$ into the energy here. We leave this term in the main manuscript to explicitly show how the total energy does scale with the size of the sheet. However, the shape of the film is determined locally through the boundary conditions at the point of contact regardless of the overall sheet size.

Before proceeding further, we will rewrite the total energy U in a slightly different way so as to subsume the inextensibility constraint and the energy density under a single integral,

$$U = \int_0^{l/2} ds \left[\frac{1}{2} B\theta'^2 + \Delta\gamma - \alpha \left(x'(s) - \cos\theta\right)\right] . \tag{7}$$

Here $x(s)$ is the horizontal coordinate of point s of the sheet. Note that the constraint written above is exactly equivalent to what is present in equation (6), as can be verified by noting that $\int_0^{l/2} ds\, x'(s) = x(l/2) - x(0) = (L - \Delta L)/2$.

To keep the upcoming computations clean, we will now denote the integrand in (7) by $\mathcal{L}(s; \theta, \theta')$ and write the integral as,

$$U = \int_0^{s_0} ds\, \mathcal{L}(s; \theta, \theta') , \tag{8}$$

where the *dependent* variable θ (and θ') appearing in the argument of $\mathcal{L}$ are considered to be functions of the *independent* variable s appearing before the semicolon. Also, s_0 is equal to $l/2$. Following [6], we will compute the first order variation of the functional (8) under shifts in the *dependent* as well as the *independent* variables. As we will see towards the end, the former will give us the governing equation for the elastica, and the later will deliver the non-trivial boundary condition of adhesion.

We subject functional (8) to a set of transformations in the *independent* and the *dependent* variable as $s \to \bar{s}$ and $\theta \to \bar{\theta}$. The transformed functional is then written as,

$$\bar{U} = \int_0^{\bar{s}_0} d\bar{s}\, \mathcal{L}(\bar{s}; \bar{\theta}, \bar{\theta}')\,, \tag{9}$$

where the transformed variable $\bar{\theta}$ is now to be considered a function of $\bar{s}$ appearing before the semicolon. Note that this transformation has also shifted the domain of integration to $\bar{s}_0$. We assume that the transformations are related by infinitesimal shifts of the form,

$$\bar{s} = s + \delta s(s)\,, \qquad \bar{\theta}(\bar{s}) = \theta(s) + \delta\theta(s)\,, \tag{10}$$

The inifinitesimal shifts above are written as functions of the untransformed variable s. These could very well be considered to be the functions of the transformed variable $\bar{s}$ since it can be shown by a short computation that up to first order $\delta\theta(\bar{s}) = \delta\theta(s)$. The δ operator here measures the total change in θ due to changes in the independent variable s, as well as changes in θ at a fixed material point. Since the two sides of $(10)_2$ are defined at different points in the space of the independent variable, the operator δ does not commute with the total derivative $()'$. Therefore, we define an operator $\tilde{\delta}$ which only measures the changes in the dependent variable θ at a fixed material label s.

$$\bar{\theta}(s) = \theta(s) + \tilde{\delta}\theta(s)\,. \tag{11}$$

Using relations (10) and (11) the two variational operators can be related as,

$$\delta\theta = \tilde{\delta}\theta + \theta'\delta s\,. \tag{12}$$

With all these definitions at hand, we write the difference between (9) and (8) as follows,

$$\bar{U} - U = \Delta U = \int_0^{\bar{s}_0} d\bar{s}\, \mathcal{L}(\bar{s}; \bar{\theta}, \bar{\theta}') - \int_0^{s_0} ds\, \mathcal{L}(s; \theta, \theta') \tag{13}$$

In order to combine the two integrals above, we need to ensure that the domains of integration of the two integrals coincide. We achieve that by transforming the shifted volume form in the first integral back to original domain and obtain the following,

$$\Delta U = \int_0^{s_0} ds\, \left[\frac{d\bar{s}}{ds}\mathcal{L}(\bar{s}; \bar{\theta}, \bar{\theta}') - \mathcal{L}(s; \theta, \theta')\right]\,, \tag{14}$$

From $(10)_1$, we note that $\frac{d\bar{s}}{ds} = 1 + \frac{d\delta s}{ds}$, and the first Lagrangian function above is Taylor expanded upto first order terms as $\mathcal{L}(s+\delta s; \theta+\delta\theta, \theta'+\delta\theta') = \mathcal{L}(s; \theta, \theta') + \frac{\partial\mathcal{L}}{\partial s}\delta s + \frac{\partial\mathcal{L}}{\partial\theta}\delta\theta + \frac{\partial\mathcal{L}}{\partial\theta'}\delta\theta'$.

Substituting these two expressions in (14), and retaining only first order terms we obtain,

$$\delta U = \int_0^{s_0} ds \left[\mathcal{L} \frac{d\delta s}{ds} + \frac{\partial \mathcal{L}}{\partial s} \delta s + \frac{\partial \mathcal{L}}{\partial \theta} \delta\theta + \frac{\partial \mathcal{L}}{\partial \theta'} \delta\theta' \right] . \tag{15}$$

We now replace the operator δ in the integrand above with $\tilde{\delta}$ using (12), and after some manipulations obtain the following,

$$\delta U = \int_0^{s_0} ds \, \frac{d}{ds} \left(\mathcal{L} \delta s \right) + \int_0^{s_0} ds \left[\frac{\partial \mathcal{L}}{\partial \theta} \tilde{\delta}\theta + \frac{\partial \mathcal{L}}{\partial \theta'} \tilde{\delta}\theta' \right] . \tag{16}$$

Note that the additional effect of varying the independent variable s is now clearly visible in the first term above. If we were only varying the dependent variable θ, as is done in standard fixed domain calculus of variation problems, then the first integral in (16) would not appear, and the two variational operators $\tilde{\delta}$ and δ would coincide. On integrating by parts the second term in the second integral on the right side of (16) we obtain the following,

$$\delta U = \int_0^{s_0} ds \, \frac{d}{ds} \left[\left(\mathcal{L} - \frac{\partial \mathcal{L}}{\partial \theta'} \theta' \right) \delta s + \frac{\partial \mathcal{L}}{\partial \theta'} \delta\theta \right] + \int_0^{s_0} ds \left[\frac{\partial \mathcal{L}}{\partial \theta} - \frac{d}{ds} \left(\frac{\partial \mathcal{L}}{\partial \theta'} \right) \right] (\delta\theta - \theta' \delta s) , \tag{17}$$

$$= \left(\mathcal{L} - \frac{\partial \mathcal{L}}{\partial \theta'} \theta' \right) \delta s \Big|_0^{s_0} + \frac{\partial \mathcal{L}}{\partial \theta'} \delta\theta \Big|_0^{s_0} + \int_0^{s_0} ds \left[\frac{\partial \mathcal{L}}{\partial \theta} - \frac{d}{ds} \left(\frac{\partial \mathcal{L}}{\partial \theta'} \right) \right] (\delta\theta - \theta' \delta s) . \tag{18}$$

Now recognising the fact that $\delta s(0) = 0$, and $\delta\theta(0) = \delta\theta(s_0) = 0$, we arrive at the following,

$$\delta U = \left(\mathcal{L} - \frac{\partial \mathcal{L}}{\partial \theta'} \theta' \right) \delta s_0 + \int_0^{s_0} ds \left[\frac{\partial \mathcal{L}}{\partial \theta} - \frac{d}{ds} \left(\frac{\partial \mathcal{L}}{\partial \theta'} \right) \right] (\delta\theta - \theta' \delta s) . \tag{19}$$

For U to be extremal, we must have $\delta U = 0$, which requires the following relations to hold for arbitrary variations in s and θ,

$$\mathcal{L} - \frac{\partial \mathcal{L}}{\partial \theta'} \theta' = 0 , \qquad \text{at } s = s_0 , \tag{20}$$

$$\left[\frac{\partial \mathcal{L}}{\partial \theta} - \frac{d}{ds} \left(\frac{\partial \mathcal{L}}{\partial \theta'} \right) \right] = 0 , \qquad \text{for } 0 < s < s_0 . \tag{21}$$

On substituting the expression for $\mathcal{L}$ from (7), we immediately see that (20) delivers the adhesion boundary condition [7], and (21) gives us the governing equation of the Euler elastica.

$$\tfrac{1}{2} B (\theta')^2 = \Delta\gamma , \tag{22}$$

$$\theta'' + (\alpha/B) \sin\theta = 0 . \tag{23}$$

IV. SOLUTIONS OF EQN. 23

Integrating Eqn. 23 once gives an expression for the curvature:

$$\theta' = \sqrt{2(P/B)\cos(\theta) + c_1} \tag{24}$$

with c_1 an integration constant. The boundary condition of Eqn. 22 allows c_1 to be determined, and the differential equation can then be solved:

$$\theta(s) = 2am\left(\sqrt{\frac{P+\Delta\gamma}{2B}}s, \sqrt{\frac{2}{1+\Delta\gamma/P}}\right), \tag{25}$$

where am is the Jacobi amplitude function. The point of contact, ℓ, can also be analytically determined:

$$\frac{\ell}{2} = F\left(-\frac{\pi}{4}, \sqrt{\frac{2}{1+\Delta\gamma/P}}\right)\sqrt{\frac{2B}{P+\Delta\gamma}}, \tag{26}$$

where F is the eliptic integral of the first kind.

V. ENERGY RELEASE RATE

The inextensible film has a mechanical energy given by:

$$U_M = 2b\int_0^{\ell/2} \frac{B}{2}(\theta')^2 \partial s, \tag{27}$$

as the fixed grips allow no contribution from work during a virtual crack displacement. Using Eqn. 24 the energy can be rewritten as:

$$U_M = 2b\int_0^{\ell/2} (P\cos(\theta) + \Delta\gamma)\partial s. \tag{28}$$

The first term of the integral results in a constant due to the inextensibility constraint, and the second integral is trivial. Hence, the total mechanical energy can be written:

$$U_M = bP(L - \Delta L) + b\ell\Delta\gamma. \tag{29}$$

The energy relase rate is given by the areal derivative of the mechanical energy. In this case the element of area is given by $\partial A = -b\partial\ell$, where the negative sign arises because ∂A is positive as the crack closes. Hence,

$$G = -\frac{\partial U_M}{b\partial\ell} = -\Delta\gamma. \tag{30}$$

As G is constant, the areal derivative of G is equal to zero.

---

[1] ASTM Standard D1876 - 08(2015)e1, *Standard Test Method for Peel Resistance of Adhesives (T-Peel Test* (ASTM International, West Conshohocken, PA, 2015).

[2] L. F. Kawashita, D. R. Moore, and J. G. Williams, Protocols for the measurement of adhesive fracture toughness by peel tests, The Journal of Adhesion **82**, 973 (2006).

[3] K. Kendall, Thin-film peeling: the elastic term, J. Phys. D: Appl. Phys. **8**, 1449 (1975).

[4] D. Maugis and M. Barquins, Fracture mechanics and the adherence of viscoelastic bodies, J. Phys. D: Appl. Phys. **11**, 1989 (1978).

[5] T. J. W. Wagner and D. Vella, The 'sticky elastica': delamination blisters beyond small deformations, Soft Matter **9**, 1025 (2013).

[6] E. L. Hill, Hamilton's principle and the conservation theorems of mathematical physics, Reviews of Modern Physics **23**, 253 (1951).

[7] C. Majidi, Remarks on formulating an adhesion problem using euler's elastica (draft), Mech. Res. Comm. **34**, 85 (2007).